



# Intracellular K<sup>+</sup> Limits T-cell Exhaustion and Preserves Antitumor Function

Camille Collier<sup>1,2</sup>, Kelly Wucherer<sup>1,2</sup>, Matthew McWhorter<sup>1,2</sup>, Chelsea Jenkins<sup>1,2</sup>, Alexandra Bartlett<sup>1,2</sup>, Rahul Roychoudhuri<sup>3</sup>, and Robert Eil<sup>1,2</sup>

## ABSTRACT

T cells are often compromised within cancers, allowing disease progression. We previously found that intratumoral elevations in extracellular K<sup>+</sup>, related to ongoing cell death, constrained CD8<sup>+</sup> T-cell Akt-mTOR signaling and effector function. To alleviate K<sup>+</sup>-mediated T-cell dysfunction, we pursued genetic means to lower intracellular K<sup>+</sup>. CD8<sup>+</sup> T cells robustly and dynamically express the Na<sup>+</sup>/K<sup>+</sup> ATPase, among other K<sup>+</sup> transporters. CRISPR-Cas9-mediated disruption of the *Atp1a1* locus lowered intracellular K<sup>+</sup> and elevated the resting membrane potential (i.e.,  $V_m$ ,  $\psi$ ). Despite compromised Ca<sup>2+</sup> influx, *Atp1a1*-deficient T cells harbored tonic hyperactivity in multiple signal transduction cas-

cades, along with a phenotype of exhaustion in mouse and human CD8<sup>+</sup> T cells. Provision of exogenous K<sup>+</sup> restored intracellular levels in *Atp1a1*-deficient T cells and prevented damaging levels of reactive oxygen species (ROS), and both antioxidant treatment and exogenous K<sup>+</sup> prevented *Atp1a1*-deficient T-cell exhaustion *in vitro*. T cells lacking *Atp1a1* had compromised persistence and antitumor activity in a syngeneic model of orthotopic murine melanoma. Translational application of these findings will require balancing the beneficial aspects of intracellular K<sup>+</sup> with the ROS-dependent nature of T-cell effector function.

*See related Spotlight by Banuelos and Borges da Silva.*

## Introduction

The past 20 years of translational oncology provide a framework in which the ability to eradicate cancer has increased in direct relation to our understanding of T-cell biology (1). Although T cells infiltrate cancers, only a small proportion of patients that receive immunotherapy achieve durable regression of disease, owing to tumor-induced suppression of T-cell function (2–4). Following T-cell receptor (TCR) engagement, naïve T cells ( $T_N$ ) progressively differentiate into stem cell memory ( $T_{SCM}$ ), central memory ( $T_{CM}$ ), effector memory ( $T_{EM}$ ), and terminally differentiated exhausted T cells ( $T_{Ex}$ ). As T cells differentiate along this continuum, transcriptional, epigenetic, and metabolic changes drive the acquisition of effector functions (IFN $\gamma$  production, cytosis) in  $T_{EM}$  cells, along with the coincident loss of stem-like behaviors (multipotency, persistence, and self-renewal) seen in  $T_{SCM}$  and  $T_{CM}$  cells (5). Within cancers, repetitive TCR stimulation drives  $T_{EM}$  cells to differentiate into  $T_{Ex}$  cells, with compromised effector functions and loss of stem-cell like behavior. In addition to  $T_{Ex}$  cell hyporesponsiveness, direct suppression of TCR signaling (i.e., PD-L1, CTLA-4) can drive T-cell intratumoral dysfunction (1, 2). We previously reported that elevated extracellular potassium ( $\uparrow [K^+]_e$ ) within tumors directly suppresses TCR-induced signal transduction and effector function (6–8). In the current work, we aimed to imbue

tumor-specific T cells with resistance to  $\uparrow [K^+]_e$  by reprogramming K<sup>+</sup> transport to result in a lower intracellular K<sup>+</sup> ( $[K^+]_i$ ).

To understand the underpinnings of T-cell K<sup>+</sup> physiology, we performed whole-transcriptomic analysis of T cells in varied states of activation and differentiation. Although our efforts and those of others have focused on the role of the K<sup>+</sup> channels K<sub>v</sub>1.3 and K<sub>Ca</sub>3.1, we also found that transcripts encoding a number of other K<sup>+</sup> channels and pumps were differentially abundant across T-cell populations (9). We elected to focus on the Na<sup>+</sup>/K<sup>+</sup> ATPase, owing to its established contribution to  $[K^+]_i$ , resting membrane potential (i.e.,  $V_m$ ), and robust expression (10). The Na<sup>+</sup>/K<sup>+</sup> ATPase exports three sodium ions and imports two potassium ions, producing a cytoplasm that is hyperkalemic and hyponatremic with a  $V_m$  of approximately -60 mV compared with the extracellular space (11). Despite depolarizing the resting  $V_m$  and compromising Ca<sup>2+</sup> influx, genetic disruption of the Na<sup>+</sup>/K<sup>+</sup> ATPase produced spontaneous activation within TCR and Akt-mTOR signaling cascades. Ongoing signal transduction resulted in  $T_{Ex}$  cell formation, mirroring other instances of tonic T-cell signaling. Mechanistically, we found *Atp1a1*-deficient T cells to be in a state of stress response, with elevated levels of reactive oxygen species (ROS). Treatment with the antioxidant N-acetylcysteine (NAC) prevented ROS accumulation and  $T_{Ex}$  cell formation *in vitro*. Yet, the driving source of dysfunction in Na<sup>+</sup>/K<sup>+</sup> ATPase deficient T cells was a depletion of  $[K^+]_i$ . Provision of  $[K^+]_e$  raised  $[K^+]_i$  levels and prevented ROS accumulation and phenotypic exhaustion. Consistent with their  $T_{Ex}$  cell phenotype, tumor-specific T cells lacking *Atp1a1* had compromised *in vivo* persistence and antitumor activity. These findings indicate that a modicum of  $[K^+]_i$  is required in T cells to prevent unregulated signal transduction in TCR and Akt-mTOR signaling, resulting in T-cell exhaustion. Future efforts will focus on understanding how  $[K^+]_i$  regulates ROS and providing T cells the abilities to weather the stressors of the tumor microenvironment, including pathologic ion concentrations. A deeper understanding of T-cell ion transport will advance cancer immunotherapy by informing the development and application of pharmacologic and genetic interventions that prevent T-cell exhaustion, while also augmenting intratumoral effector functions.

<sup>1</sup>Division of Surgical Oncology, Department of Surgery, Oregon Health & Science University, Portland, Oregon. <sup>2</sup>Department of Cell, Developmental, & Cancer Biology, Knight Cancer Institute, Oregon Health & Science University, Portland, Oregon. <sup>3</sup>Department of Pathology, University of Cambridge, Cambridge, United Kingdom.

**Corresponding Author:** Robert Eil, Oregon Health & Science University, 3181 SW Sam Jackson Park Road, Portland, Oregon, 97239. E-mail: eil@ohsu.edu

Cancer Immunol Res 2023;XX:XX–XX

doi: 10.1158/2326-6066.CIR-23-0319

This open access article is distributed under the Creative Commons Attribution-NonCommercial-NoDerivatives 4.0 International (CC BY-NC-ND 4.0) license.

©2023 The Authors; Published by the American Association for Cancer Research

## Materials and Methods

### Study approval

All mouse experiments were approved by the Animal Care and Use Committee at OHSU (Department of Comparative Medicine). All infectious agents were approved by the OHSU Institutional Biosafety Committee. Deidentified healthy donors (HD) were recruited and enrolled by the Oregon Clinical and Translational Research Institute under the Research Volunteer Repository program.

### Mice

All mice were obtained from The Jackson Laboratory. C57BL/6 mice (Cat. 000664) of 6–8 weeks of age were used as recipient hosts for adoptive transfer, unless otherwise indicated. OT-1 Ly5.1 transgenic mice were used for adoptive cell transfer (ACT) and viral kinetics experiments. To obtain OT-1 Ly5.1 mice (CD45.1/1<sup>+</sup>), we crossed OT-1 Ly5.2 (CD45.2/2<sup>+</sup>) mice (C57BL/6-Tg (TcraTcrb) 1100Mjb/J; Cat. 003831) with Ly5.1 (CD45.1/1<sup>+</sup>) mice (B6.SJL-PtprcaPepcb/BoyJ; 002014). This resulted in OT-1 mice heterogeneous for Ly5.1 (CD45.1/2<sup>+</sup>), which were further crossed to obtain OT-1 Ly5.1 homozygotes. We bred OT-1 mice with Rag2<sup>-/-</sup> mice (B6.Cg-Rag2tm1.1gGn/J; Cat. 008449) to obtain OT-1 Rag2<sup>-/-</sup> progeny. All mice were maintained under specific pathogen-free conditions.

### Cell and virus lines

B16-OVA was generated from parental B16-F10 (obtained from the ATCC, Cat no. CRL-6475 in 2020). B16-F10 was transduced with MSCV γ-retroviral particles encoding a full-length ovalbumin (OVA) protein in tandem with a T2A sequence and a blasticidin resistance insert. B16-OVA-T2A blasticidin-resistant transductants were selected by supplementing culture medium with 10 µg/mL Blasticidin S HCl (Gibco). The reactivity of OT-1 CD8<sup>+</sup> T cells against the selected B16-OVA-T2A tumor line was validated using a coculture. Briefly, B16-OVA cells were pretreated overnight with 50 µg/mL recombinant murine IFNγ (PeproTech). A total of 5×10<sup>5</sup> parental B16 or engineered B16-OVA cells were coincubated with an equal number of OT-1 CD8<sup>+</sup> T cells in complete RPMI-1640 (see below) supplemented with 100 IU/mL recombinant human IL2 (PeproTech) for 6 hours at 37°C 5% CO<sub>2</sub>. All cells were then fixed and processed to assess cytokine production of OVA-reactive OT-1 T cells by flow (see “flow cytometry”). Cell lines were maintained in complete media DMEM (Gibco) completed with 10% FBS (VWR), 1% glutamine (Gibco), 1% non-essential amino acids (Gibco), 1% penicillin-streptomycin (Gibco), 500 ng/mL amphotericin B (Gibco) and 1X Plasmocin Prophylaxis (Invivogen). B16-OVA cells were maintained in 10 µg/mL blasticidin. All cell lines are tested for mycoplasma via a PCR-based assay approximately once a week when in use. Vaccinia virus expressing the OVA epitope was a generous gift from Jeffery Nolz (OHSU – MMI). vv-OVA was generated by homologous recombination, where DNA encoding an OVA epitope was inserted into the TK gene of the parental strain of the vaccinia virus (Western Reserve) and selected by lack of TK activity. The vv-OVA strain was maintained by propagation in BSC-40 cells.

### Isolation of naïve T cells from spleens or whole blood

Murine CD8<sup>+</sup> T cells were isolated from the spleens of OT-1 Ly5.1 transgenic mice using the EasySep Mouse CD8<sup>+</sup> T-cell Isolation Kit (Stemcell). Spleens were first dissociated into a single-cell suspensions by mashing them and passing them through a 40 µmol/L filter, lysing for 30 seconds at room temperature using 1 mL ACK lysis buffer

(Gibco), and then the resultant splenocytes were resuspended into EasySep Buffer (Stemcell) as per the manufacturer’s instructions. CD8<sup>+</sup> T cells were isolated via negative selection using an EasyEights EasySep Magnet (Stemcell), which yielded an enrichment of 96%–100% purity. Human CD4<sup>+</sup> and CD8<sup>+</sup> HD T cells were purified from fresh whole-blood via gradient with Ficoll-Paque PLUS Media (Cytiva). Briefly, 2 mL of blood were diluted 1:1 with Ca<sup>2+</sup>- and Mg<sup>2+</sup>-free DBPS (Gibco), and then interfaced with 3 mL of ficoll media in a 50 mL conical. These quantities were scaled according to the total volume of the sample. The interfaced sample was then centrifuged for 30 minutes at room temperature with an acceleration of 3 and the brake turned off. Finally, lymphocytes were collected from the resultant plasma–ficoll interface, where this fraction contained 60% CD45<sup>+</sup>CD4<sup>+</sup> or CD45<sup>+</sup>CD8<sup>+</sup> T cells.

### In vitro activation and culture of T cells

CD8<sup>+</sup> T cells from OT-1 mouse spleens were stimulated *in vitro* with plate-bound anti-CD3 and anti-CD28 (5 µg/mL; BioXcell) for 24 hours and expanded in RPMI-1640 (Gibco) completed with 10% FBS (Gibco), 1% nonessential amino acids (Gibco), 1% sodium pyruvate (Gibco), 1% penicillin/streptomycin (Gibco), 57 µmol/L 2-BME (Sigma), and 100 IU/mL of recombinant human (rh)IL2 (Peprotech). Mouse T cells that underwent a second 24-hour stimulation 6 days after the first stimulation are identified in the text as “serially” TCR stimulated. Isolated human T cells were stimulated *in vitro* for 48 hours in 50:50 complete RPMI-1640 (Gibco): OpTmizer CTS (Gibco) containing a 1:100 titer of TransAct (Miltenyi Biotec), 5% FBS, and 300 IU/mL of rhIL2 (Peprotech). Following stimulation with TransAct, Human T cells were maintained in 50:50 complete RPMI-1640 (Gibco): OpTmizer CTS (Gibco) 300 IU/mL of rhIL2 (Peprotech). Human T cells were exposed to 50 nmol/L ouabain (Sigma) as indicated. For antioxidant treatment, cells were cultured with 10 mmol/L NAC (Sigma). For measuring T-cell effector function, cells were washed of their original culture media (experimental or control and cytokines) before stimulation for 5 hours with anti-CD3 and anti-CD28 or with 50 ng/mL PMA (Sigma) and 1.5 µmol/L ionomycin (Sigma), without IL2, and in the presence of brefeldin A and monensin (BD Biosciences). One of these 6-hour anti-CD3 and anti-CD28 stimulation treatments is identified in the text as an “acute” TCR stimulation.

### Retroviral transduction

Platinum-E ecotropic packaging cells (Cell Biolabs; Cat. RV-101) were plated one day before transfections on poly-D-lysine-coated 10-cm plates (Corning) at a concentration of a total of 6 × 10<sup>6</sup> cells per plate. Packaging cells were transfected with 20 µg of plasmid DNA containing indicated genes of interest synthesized by Genscript, Inc. and cloned in an MSCV derived γ-retrovirus backbone derived from Addgene Plasmid #122727 along with 3 µg pCL-Eco plasmid DNA (Addgene, Plasmid #12371), using 60 µL Lipofectamine 2000 in OptiMEM (Invitrogen) where indicated, for 8 hours in antibiotic-free complete DMEM. MSCV K<sub>v</sub>1.3\_DN was obtained by site directed mutagenesis performed by Genscript, Inc. of K<sub>v</sub>1.3\_WT (6) to mutate glycine residues 399 and 401 to alanines (GYG to AYA). MSCV K<sub>v</sub>2.1 was generated by codon-optimized (jcat.de) synthesis of the wild-type *mus musculus* amino acid sequence (P35561) and EcoRI-NcoI-based digestion and ligation into MSCV by Genscript, Inc. Medium was replaced 24 hours after transfection, and cells were incubated for a further 48 hours. Retroviral supernatants were then collected and centrifuged at 2,000 x g for 2 hours at 32°C in 24-well, non-tissue culture-treated plates coated overnight in Retronectin (Takara Bio) or

spinfected for 90 minutes at 32°C in 1 µcg mL<sup>-1</sup> polybrene (Sigma), which was then removed after an additional 4-hour incubation.

### CRISPR-Cas9-mediated *Atp1a1* deletion and INDEL assessment

Non-targeting control single-guide (sg)RNA and *Atp1a1*-targeted modified sgRNAs were purchased from and synthesized by Synthego. Modified sgRNAs were designed to target protein-coding loci of the *Mus musculus* *Atp1a1* gene (Genbank #AC127357.5) and *Homo sapiens* *ATP1A1* gene (Genbank #AH001423.2). Modified sgRNAs were mixed in equal parts (murine *Atp1a1* sgRNAs: 5'-AAAAGCC-UCCAAGAGCUGC-3', 5'-GAGGGGGUGUGAGGGCGUUG-3', 5'-CUUGCAGGUGUUAAUCCCUG-3'; human *ATP1A1* sgRNAs: 5'-UGCUCGUGCAGCUGAGAUCC-3', 5'-CCAUUCAGGAGUA-GUGGGAG-3', 5'-UGGAGCGAUUCUUUGUUUCU-3'). Mixtures of complexed sgRNA and Cas9 (0.3 nmol synthetic sgRNA + 62 µmol Cas9 nuclease (Integrated DNA Technologies) and a total of 2–10×10<sup>6</sup> enriched murine CD8<sup>+</sup> T cells or human PBMCs following FICOLL density centrifugation were suspended in 25 µL of P3 electroporation buffer (Lonza) and electroporated using the Lonza 4D Nucleofector (pulse code DN100). Cells were activated *ex vivo* as above and collected for INDEL assessment on day 4 of culture.

For INDEL assessment, genomic (g)DNA was harvested from mouse and human cells at time of analysis using the DNeasy Blood and Tissue DNA kit (Qiagen), and the region containing the *Atp1a1*/*ATP1A1* sgRNA target was PCR-amplified and Sanger sequenced by Eurofins Genomics. For murine samples, a 435-bp region was amplified for sequencing (forward primer: 5'-AGCA-GAATGACCCAGAGTGG-3', reverse: 5'-GGGGGAGTTAACAG-GCTTC-3'); for human samples, a 498-bp region was amplified (forward: 5'-GTGGGGACTGGCTCATCAG-3', reverse: 5'-GAGTT-CATAACCATTAAAGTAATGAGTGG-3'). 100 to 200 ng of each amplicon was sent for sequencing with 2 pmol of its respective sequencing primer (mouse: 5'-GAGAAGAAGGGACAATGTGA-GCAG-3'; human: 5'-AGTTCATACCATTAAAGTAATGAGTGG-TAA-3'). Genomic fragments were analyzed using a 3730xl DNA Analyzer (Applied Biosystems). The indel percentage of amplicons derived from *Atp1a1*-deficient cells was deduced using the Synthego ICE tool (Synthego Performance Analysis, ICE Analysis. 2019. v3.0. Synthego).

### Intracellular cytokine staining, phosflow, flow cytometry, and FACS

For all flow cytometry experiments, T cells were stained with a fixable live/dead stain (Invitrogen) in PBS, followed by surface antibody staining (see Supplementary Table 1 unless otherwise indicated) in FACS buffer (PBS with 0.5% BSA and 0.1% sodium azide, Sigma) for 30 minutes at 4°C. For intracellular cytokine staining, cells were first stained for surface markers and then stained for intracellular molecules overnight following fixation and permeabilization following the manufacturer's protocols (BD Cytofix/Cytoperm). All antibodies were diluted in 1:200 for staining, except for phosflow antibodies (pS6<sup>S235/6</sup> PE-Cy7, pAKT<sup>S473</sup> AF488, pERK<sup>T202/Y204</sup> Pacific Blue (Cell Signaling Technology), and pCD3<sup>Y142</sup> PE (BD Biosciences), which were diluted in 1:400 pCD3<sup>Y142</sup> PE (BD Biosciences).

For phosflow, T cells were incubated with 5 µcg mL<sup>-1</sup> anti-CD3 (145-2C11) and anti-CD28-biotin (37.51) conjugates (eBioscience). TCR cross-linking was carried out at 37°C by the addition of soluble streptavidin (Thermo Fisher Scientific) to a final concentration of 20 µcg mL<sup>-1</sup>. Reactions were quenched at specified time points by the addition of warmed lyse/fix PhosFlow Buffer I (BD Biosciences). Cells were then washed and permeabilized with -80°C PhosFlow Buffer III

(BD Biosciences). After washing, cells were stained with phosphoantibodies (Supplementary Table 1) purchased from Cell Signaling Technology or BD Biosciences at a concentration of 1:400 for 1 hour. All experiments were conducted on a BD (Becton Dickinson) Fortessa or Cytek Biosciences Aurora cytometer and analyzed with FlowJo software (Tree Star, Inc.).

FACS purification of CD44<sup>-</sup>CD62L<sup>+</sup> CD8<sup>+</sup> T<sub>N</sub> and CD44<sup>+</sup>CD62L<sup>-</sup> T<sub>EM</sub> cells from the spleens of donor *Rag2*<sup>-/-</sup>CD45.2<sup>+</sup> mice and CD45.1<sup>+</sup> recipient mice was performed on a BD FACS Aria. In all instances, spleens were harvested and dissociated into a single-cell solution as previously described, then stained for viability with propidium iodide and for CD8, CD44, and CD62 L (Supplementary Table 1). Purification of CD45.2<sup>+</sup> donor cells from CD45.1<sup>+</sup> recipient mice additionally required staining of CD45.1 and CD45.2. Following a wash and resuspension in FACS buffer, live, CD19<sup>-</sup>, CD8<sup>+</sup> T cells were gated and sorted into T<sub>N</sub> (CD44<sup>-</sup>CD62L<sup>+</sup>) and/or T<sub>EM</sub> (CD44<sup>+</sup>CD62L<sup>-</sup>) populations. These populations were additionally gated on CD45.2 during FACS purification of CD45.2<sup>+</sup> OT-1 donor cells from CD45.1<sup>+</sup> recipients. In both experiments, the T<sub>N</sub> fraction had 99.9% purity upon validating the sorted fractions; the T<sub>EM</sub> fraction had 98.6% purity.

### Assessment of intracellular ROS, [K<sup>+</sup>]<sub>i</sub>, and V<sub>m</sub>

Murine CD8<sup>+</sup> T cells purified from spleens were rested in IL2-free complete RPMI-1640 (as defined above) for 16 to 18 hours. Cells were stained with fixable live/dead and anti-CD8 (Supplementary Table 1), washed, and then resuspended with 5 µmol/L DiSBAC<sub>2</sub> (ref. 3; Invitrogen), 2.5 µmol/L DCFDA (AdipoGen Life Sciences), or 1 µmol/L APG-4 (Asante Green-4, TEFLabs) in complete RPMI-1640 and incubated for 30, 20, and 90 minutes at room temperature, respectively. Cells stained for oxonol were additionally stained for a Thy1.1 transduction marker, washed 1X and analyzed by flow cytometry. Only cells that were gated as live and CD8<sup>+</sup> and, as necessary, Thy1.1<sup>+</sup> were assessed for relative V<sub>m</sub>. DCFDA- and APG-4-loaded cells were analyzed on a cytometer immediately after incubation without washing. For these assays, live, singlet CD8<sup>+</sup> T cells were assessed for relative ROS abundance and intracellular [K<sup>+</sup>], respectively.

For determination of [K<sup>+</sup>]<sub>i</sub>, we generated standard curves representing induced [K<sup>+</sup>]<sub>i</sub> versus APG-4 mean fluorescence intensity (MFI) and used these standard curves to compute [K<sup>+</sup>]<sub>i</sub> for each cell type. Briefly, standard curves accommodated [K<sup>+</sup>]<sub>i</sub> ranging from 0 to 143 mmol/L, where these [K<sup>+</sup>]<sub>i</sub> were induced by incubating cells with isotonic, [K<sup>+</sup>]-controlled RPMI-1640, 1 µmol/L APG-4 (pre-incubated 1:1 with Pluronic-127, Invitrogen), and K<sup>+</sup>-permeable ionophores valinomycin, gramicidin, and nigericin (Sigma) at 10 µmol/L, along with 50 mmol/L D-sucrose (Thermo Fisher Scientific) to normalize cell size. Cells queried for [K<sup>+</sup>]<sub>i</sub> were incubated with APG-4 and isotonic, K<sup>+</sup>-free RPMI-1640 and live, CD8<sup>+</sup> T cells were analyzed via flow cytometry. After flow analysis, we established linear regressions ( $r^2 \geq 0.80$ ) to deduce [K<sup>+</sup>]<sub>i</sub> of the queried sample. Standard curves were generated for each unique cell type (i.e., *Atp1a1*-deficient cells, *Atp1a1*-sufficient cells).

For V<sub>m</sub> and [K<sup>+</sup>]<sub>i</sub> assessment, to control for technical variations in dye loading, a fluorometrically distinguishable loading control was included within each sample, typically a murine CD8<sup>+</sup> T-cell retrovirally transduced to express Thy1.1 and stained CD90.1 PE-Cy7 (BD Biosciences). The quotient between the dye's MFI of experimental cells and loading control cells is depicted as relative MFI. The "Relative MFI" for both "Vehicle" and "K<sup>+</sup> 20 mmol/L" was determined using the average of "Vehicle" replicates as the denominator.

### TCR-induced calcium influx

Murine CD8<sup>+</sup> T cells were isolated from spleens and primed as above. Before analysis, cells were rested in IL2-free complete RPMI-1640 for at least 8 hours. Cells were loaded with 1 μmol/L Fluo3-AM and 1 μmol/L Fura Red-AM (Invitrogen) for 30 minutes at 37°C in HBSS with 1.26 mmol/L Ca<sup>2+</sup>, 0.90 mmol/L Mg<sup>2+</sup> and 2% FCS (Sigma), washed twice, and then resuspended in HBSS with 10 μg/mL anti-CD3 (145-2C11) and anti-CD28-biotin (37.51) conjugates (eBioscience), a live/dead stain and anti-CD8 (Supplementary Table 1). For flow cytometry analysis, samples were resuspended in 37°C additive-free RPMI, a baseline measurement was recorded for 20 seconds, followed by the addition of streptavidin (Invitrogen) to a final concentration of 20 μg mL<sup>-1</sup> to induce TCR cross-linking and Ca<sup>2+</sup> influx. The BD Fortessa cytometer was used for the calcium influx assay. Kinetic analyses were performed with the FlowJo software package (TreeStar) and are gated on live CD8<sup>+</sup> T cells.

### ACT and tumor immunotherapy

We implanted C57BL/6 with subcutaneous B16-OVA melanoma ( $1 \times 10^6$  cells). At the time of ACT, 10 days after tumor implantation, mice ( $n \geq 5$  for all groups) were sub-lethally irradiated (500 cGy, XStrahl CIX2), randomized, and injected intravenously with a total of  $2 \times 10^6$  OT-1 Ly5.1 cells electroporated with scrambled sgRNA or Atp1a1-sgRNA. A third group was injected intravenously with 100 μL of PBS as a nontreatment control. Mice used to assess tumor-infiltrating lymphocytes (TIL) 5 to 7 days after transfer were intravenously injected with a mixture containing a total of  $6 \times 10^5$  OT-1 ( $3 \times 10^5$  of Scramble/Atp1a1 sgRNA treated each) cells total. Both cohorts received intraperitoneal injections of rhIL2 in PBS ( $5 \times 10^4$  IU in 0.5 mL) once daily for 2 days starting on the day of cell transfer. Mice supplemented with NAC were additionally administered with intraperitoneal injections of NAC at a dosage of 0.25 mg/g once daily until the study's endpoint. NAC intraperitoneal injections were prepared in PBS, neutralized to pH = 7.2–7.8, and sterile-filtered before administration. For longitudinal tumor curve studies, tumors were measured using digital calipers every 2–3 days for 28–35 days. Size was measured in a blinded fashion approximately every two days after transfer, and tumor area was calculated as length × width of the tumor. Mice with tumors greater than 400 mm<sup>2</sup> were euthanized. The products of the perpendicular tumor diameters are presented as mean ± s.e.m. at the indicated times after ACT.

For administration of *Rag2*<sup>-/-</sup>CD45.2<sup>+</sup> OT-1 T<sub>N</sub> and VV-OVA to CD45.1<sup>+</sup>, CD45.2<sup>+</sup> T<sub>N</sub> cells were immediately prepared for transfer after FACS purification at a dosage of a total of  $5 \times 10^4$  cells per CD45.1<sup>+</sup> recipient. These donor cells were administered via intravenous injection.

### TIL processing and analysis

B16-OVA tumors were analyzed for infiltrate of transferred cells to B16 tumors and spleens 5 to 7 days after ACT. Mice whose splenocytes and TILs were interrogated for *in vivo* IFNγ production were administered 100 μg Brefeldin A (Sigma) in PBS via retro-orbital injection 4 to 6 hours before euthanasia and tissue processing. Following euthanasia, tumors and spleens were promptly dissected, weighed, and stored in ice-cold PBS until further processing. Tumors were subsequently minced with surgical scissors, suspended into 3 mL of ice-cold PBS, dissociated into a single-cell solution using a GentleMACS octo-dissociator with heaters (Miltenyi Biotec, program = m\_impTumor\_03), filtered through a

100 μmol/L filter, and then consolidated and processed for flow cytometry (see above). Spleens were mashed and filtered through a 40 μmol/L filter, ACK lysed for 30 seconds using ACK lysing buffer (Gibco), and then consolidated and processed for analysis by flow cytometry. All B16-OVA tumor samples were stained with, at minimum, fixable live/dead, CD8, CD90.2, CD45.1, and CD45.2, along with phenotypic PD1 and CD62 L (Supplementary Table 1). B16-OVA tumors were analyzed on a Cytek Aurora spectral cytometer. Analyzed TILs are gated on a live, CD90.2<sup>+</sup>CD8<sup>+</sup> population, and transferred populations are additionally congenically distinguished from endogenous CD90.2<sup>+</sup>CD8<sup>+</sup> cells via CD45.1 and CD45.2.

Following flow cytometry and analysis, the relative abundance of co-transferred cells was corrected for all enumerative statistics (e.g., "%CD45.1<sup>+</sup> of CD8<sup>+</sup>") using the composition of the adoptively transferred cell mixture. Briefly, we assessed the input mixtures for relative abundance of each congenically marked, transferred cell type (i.e., CD45.1/2<sup>+</sup> and CD45.1/1<sup>+</sup> cells). These abundances were then used to assign a corrective constant to each component of the mixture, where the "major" component of the mixture was provided a constant of 1 and the "minor" component was assigned a constant of greater than 1. Following tumor harvest and flow cytometry, the observed abundances of TILs were corrected by multiplying these constants with the observed abundances. Statistics that represent a percentage of a whole (e.g., "%CD45.1/2<sup>+</sup> of CD45.1<sup>+</sup> cells") were then further corrected to reflect both the corrected relative abundances of CD45.1/2<sup>+</sup> and CD45.1/1<sup>+</sup> cells at the time of transfer and the total component of the whole that both parts occupy.

### RNA sequencing and analysis

RNA sequencing (RNA-seq) and determination of differentially expressed genes was performed by Azenta Life Sciences. Briefly, RNA was extracted from frozen murine CD8<sup>+</sup> T-cell pellets using the RNeasy Plus Universal Mini Kit (Qiagen) as per the manufacturer's instructions. RNA integrity was checked using TapeStation (Agilent Technologies), and sequencing libraries were prepared using the NEBNext Ultra II RNA Library Prep for Illumina (New England Biolabs) following the manufacturer's instructions. Briefly, mRNAs were first enriched using Oligo(dT) beads. Following mRNA fragmentation for 15 minutes at 94°C, first and second strand cDNA was synthesized using NEBNext Random Primers (New England Biolabs). cDNA fragments were end-repaired, adenylated at 3' ends, ligated to NEBNext Adapters (New England Biolabs), and enriched by PCR. Samples were clustered onto a flowcell and sequenced on the Illumina hiSeq 4000 (Illumina) with a total of  $2 \times 150$  bp paired end reads. Base-calling and raw sequence data were de-multiplexed using Illumina's CASAVA and bcl2fastq 2.20 software. Sequenced reads were trimmed using Trimmomatic v.0.36 (USADEL LAB, usadelab.org) and aligned to the mouse genome (ENSEMBL GRCm39) using the STAR aligner v.2.5.2b. Unique gene hit counts were deduced using the Subread package v.1.5.2, and only reads that fell within exon regions were retained for analysis. Differentially expressed genes were calculated using the R DESeq2 package. The Fisher's exact test or *t* test was used to evaluate significance with indicated *P* value and fold-change thresholds. Gene set enrichment analysis (GSEA) was carried out using GSEA v4.2.3 software with enrichment of the MSigDB hallmark gene set (12, 13).

### Immunoblot analysis

CD8<sup>+</sup> murine T cells or human lymphocytes were resuspended in 50–100 μL cell lysis buffer composed of 5 mL Mammalian Protein

Extraction Reagent (Thermo Fisher Scientific), 50 μL Protease Inhibitor (Bimake), and 50 μL Phosphatase Inhibitors A and B (Bimake). Samples were then centrifuged at 20,000 × g for 10 minutes at 4°C to pellet cell debris. Proteins were extracted from the supernatant by adding NuPAGE LDS Sample Buffer (Thermo Fisher Scientific) supplemented with 5% 2-BME (Sigma) and heating the sample for 10 minutes at 75°C. Protein content was then quantified using the Pierce BCA Protein Assay Kit (Thermo Fisher Scientific), a fluorometric plate assay that used to generate an absorbance versus protein concentration standard curve and subsequently extrapolate protein concentration from extracts. Between 15 and 25 μg proteins were separated by 4%–12% SDS-PAGE, followed by standard immunoblot analysis using anti-Na<sup>+</sup>-K<sup>+</sup>-ATPase α1 (for mouse cells, Cell Signaling Technology #23565) at 1:1,000, anti-Na-K-ATPase (for human cells, Cell Signaling Technology #3010) at 1:1,000 or anti-GAPDH (as a loading control, Cell Signaling Technology) at 1:5,000 at 4°C overnight. Detection of proteins was performed using secondary antibodies conjugated to horseradish peroxidase, incubated at 1:5,000 for 1 hour at room temperature, and developed using the super signal west pico chemiluminescent substrate (Thermo Fisher Scientific). Blots were imaged on a GelDoc XR+ imager with Image Lab software (Bio-Rad).

### Statistical analysis

Data were analyzed using an unpaired two-tailed Student *t* tests or two-way ANOVA. For adoptive transfer experiments, recipient mice were randomized before cell transfer. Tumor measurements were captured in a blinded fashion and plotted as the mean ± SEM for each data point. Tumor treatment graphs were compared by using the Wilcoxon rank sum test, and analysis of animal survival was assessed using a log-rank test. In all cases, two-tailed tests with *P* values less than 0.05 were considered significant. Statistics were calculated using GraphPad Prism 7 software (GraphPad Software Inc). Experimental sample sizes were chosen using power calculations, preliminary experiments, or were based on previous experience of variability in similar experiments. Samples that had undergone technical failure during processing were excluded from subsequent analysis.

### Data availability

RNA-seq data are available at GEO, accession numbers GSE242525 and GSE84996. Raw data for Fig. 1C were generated at the NIH Intramural Sequencing Center, and the derived data are available from the corresponding author upon request. Sequencing of genomic DNA for quantification of insertion and deletion frequencies can be accessed via Genbank Accession numbers OR795845-66.

## Results

### Cell-intrinsic regulators of T-cell ion transport

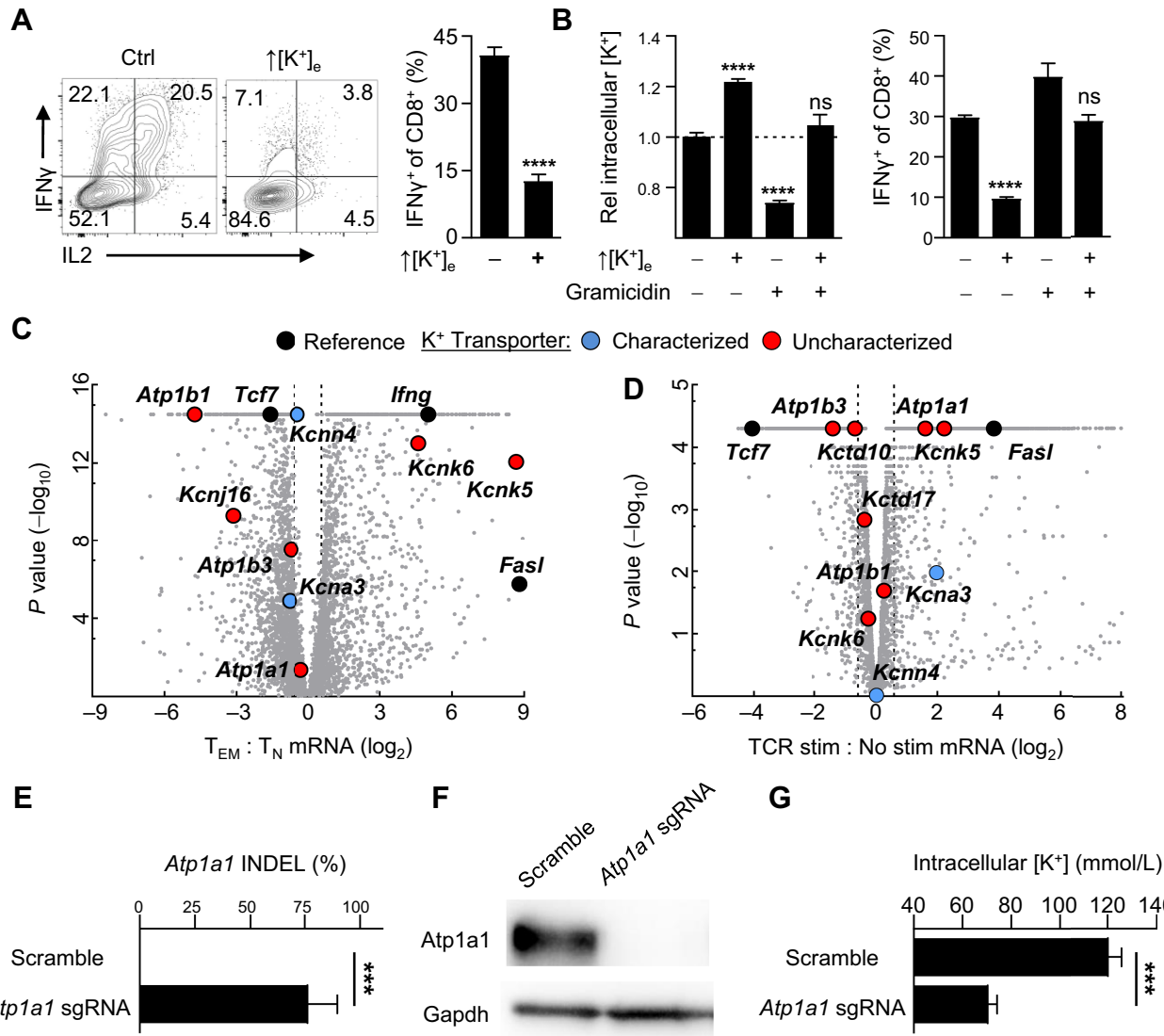
We previously found that cancer cell death results in accumulation of K<sup>+</sup> within the extracellular space of tumors, constraining mouse and human T-cell activation (6, 14). Here, we found that ↑[K<sup>+</sup>]<sub>e</sub>, characteristic of tumors, suppressed cytokine production in response to TCR ligation in CD8<sup>+</sup> T cells (Fig. 1A). In addition, ↑[K<sup>+</sup>]<sub>e</sub> promoted T-cell suppression via elevation in [K<sup>+</sup>]<sub>i</sub>, quantified by the fluorescence of the K<sup>+</sup>-sensitive dye APG-4, which could be reversed with the addition of the ionophore gramicidin (Fig. 1B). Gramicidin creates synthetic pores in the plasma membrane that are permeable to Na<sup>+</sup> and K<sup>+</sup>, lowering [K<sup>+</sup>]<sub>i</sub>, depolarizing *V<sub>m</sub>* and restoring cytokine production in the presence of ↑[K<sup>+</sup>]<sub>e</sub> (6).

To obtain a holistic understanding of K<sup>+</sup> transporters in T cells, we FACS isolated naïve (T<sub>N</sub>) CD44<sup>+</sup> CD62L<sup>+</sup> CD8<sup>+</sup> T cells from OT-I TCR transgenic *Rag2*<sup>-/-</sup>CD45.2<sup>+</sup> mice and transferred them to CD45.1<sup>+</sup> hosts in combination with OVA-expressing vaccinia virus (VV-OVA). We then purified T<sub>N</sub> (CD44<sup>+</sup>CD62L<sup>+</sup>) and T<sub>EM</sub> (CD44<sup>+</sup>CD62L<sup>-</sup>) populations from the recipients and performed whole-transcriptomic analysis (Fig. 1C). Similarly, we activated CD8<sup>+</sup> T cells for 2 hours via their TCR and assessed global transcriptional changes (Fig. 1D). We found high expression of transcripts encoding the channels K<sub>v</sub>1.3 and K<sub>Ca</sub>3.1, as expected. In addition, multiple other voltage gated, ligand gated, two-pore, and inwardly rectifying channels, along with alpha and beta subunits of the Na<sup>+</sup>/K<sup>+</sup> ATPase, were differentially expressed across CD8<sup>+</sup> T-cell subset and state. Drawing from these findings, we elected to interrogate the role of the Na<sup>+</sup>/K<sup>+</sup> ATPase in CD8<sup>+</sup> T cells, owing to its abundance and dynamism in CD8<sup>+</sup> T cells, along with its importance in other cell types that maintain high intracellular [K<sup>+</sup>] (15).

### The Na<sup>+</sup>-K<sup>+</sup>-ATPase is required for T-cell quiescence

The Na<sup>+</sup>/K<sup>+</sup> ATPase is a heterodimeric enzyme consisting of catalytic (alpha) and regulatory (beta) subunits (15). Because both *Atp1b1* and *Atp1b3* isoforms of the β-subunit are present in CD8<sup>+</sup> T cells, we targeted the nonredundant α isoform, encoded by the *Atp1a1* locus, for genetic disruption (Fig. 1E and F). Using the fluorometric K<sup>+</sup> dye APG-4, we found that CD8<sup>+</sup> T cells lacking the Na<sup>+</sup>/K<sup>+</sup> ATPase harbored an intracellular [K<sup>+</sup>]<sub>i</sub> of 70.6±6 versus 130.8±9 mmol/L in control cells (Fig. 1G). In addition to maintaining [K<sup>+</sup>]<sub>i</sub>, the Na<sup>+</sup>/K<sup>+</sup> ATPase supports a negative resting *V<sub>m</sub>* relative to the extracellular space (15). We used the voltage-sensitive membrane-permeable dye DiSBAC<sub>2</sub> (3), to comparatively assess membrane potential between CD8<sup>+</sup> T-cell populations. As expected, T cells deficient for *Atp1a1* maintained a depolarized *V<sub>m</sub>* compared with scramble controls. CD8<sup>+</sup> T cells transduced with retroviral particles encoding K<sup>+</sup> channels that enforce a more negative membrane potential, that is, hyperpolarization (K<sub>ir</sub>2.1 over expression), or increase the membrane potential closer to zero, depolarization (dominant negative K<sub>v</sub>1.3), are included for comparison and assay validation (Fig. 2A). Concordantly, we found that *Atp1a1* disruption compromised Ca<sup>2+</sup> influx following both TCR- and ionomycin-induced store operated calcium entry (Fig. 2B and C). Yet, CD8<sup>+</sup> T cells lacking the Na<sup>+</sup>/K<sup>+</sup> ATPase had abundant phosphorylation within a number of signal transduction pathways. Most notably, CD3ζ sustained high levels of phosphorylation, along with Akt-mTOR and MAPK/Erk pathway members (Fig. 2D). Consistent with increased activation within multiple signaling cascades, *Atp1a1*-deficient CD8<sup>+</sup> T cells harbored high expression of activation and exhaustion markers, such as PD-1, Tim-3, Fas, and CD69, with a relative loss of the stemness-associated proteins Tcf7 and CD62 L (Fig. 2E and F). *Atp1a1*-deficient T cells also exhibited diminished effector function (Fig. 2G; refs. 16–18).

Despite contributing to a resting negative *V<sub>m</sub>*, and therefore promoting TCR-induced Ca<sup>2+</sup> influx, the primarily role of the Na<sup>+</sup>/K<sup>+</sup> ATPase in T cells is to constrain tonic signal transduction that otherwise disrupts T-cell quiescence and promotes T<sub>Ex</sub> cell formation (19, 20). To better understand how the Na<sup>+</sup>/K<sup>+</sup> ATPase controlled T-cell behavior, we first performed whole-transcriptomic analysis of C57BL/6 CD8<sup>+</sup> T cells four days after CRISPR-Cas9-mediated disruption of *Atp1a1*. Transcriptionally, *Atp1a1* disruption promoted effector T-cell programs, stress response pathways, and anabolic metabolism, with a coincident loss of stemness-associated programs (Fig. 3A and B). GSEA of expression profiles increased

**Figure 1.**

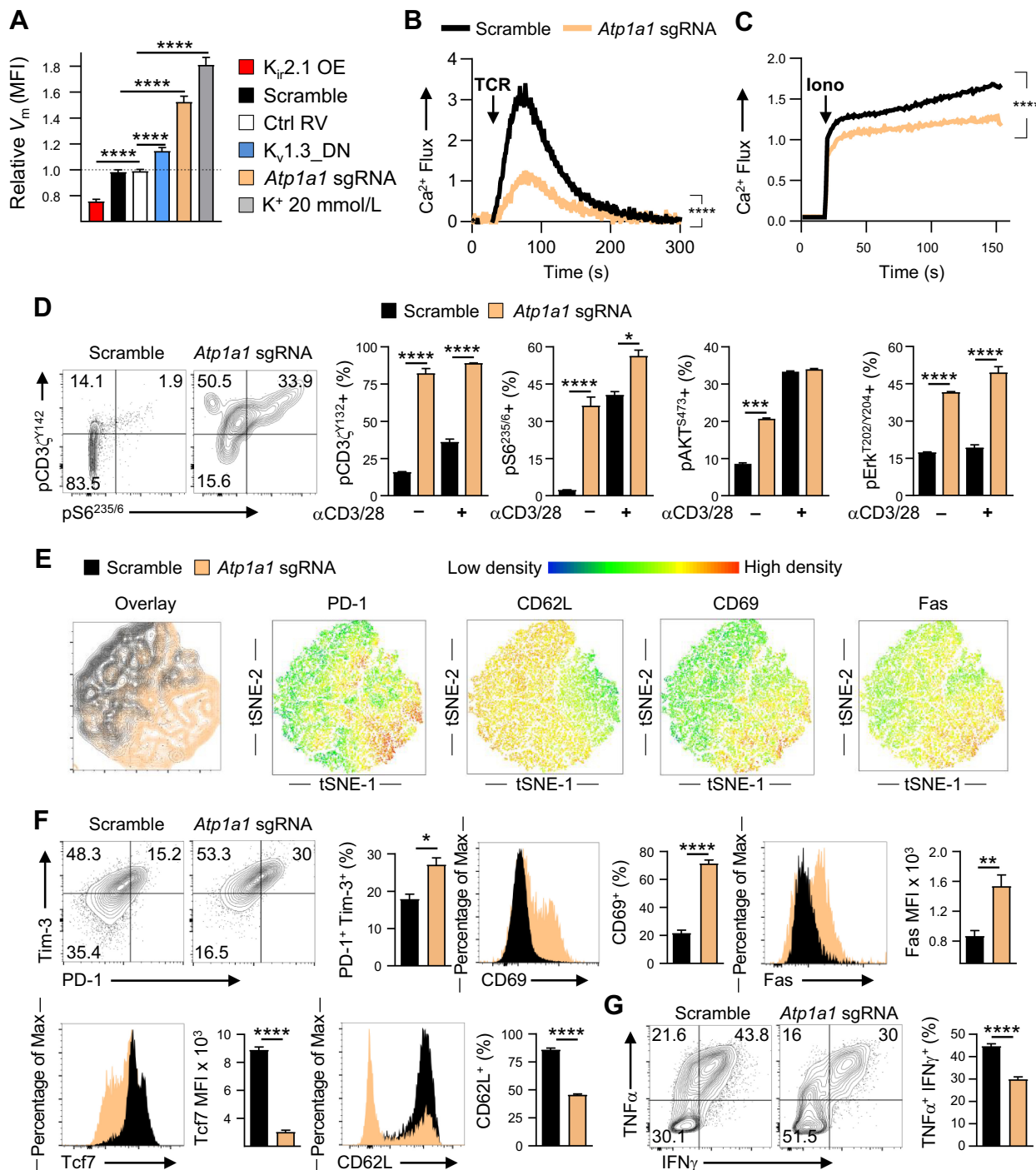
Elevated extracellular K $^+$  in tumors suppresses T-cell function via increasing intracellular levels. **A**, Representative flow cytometry plots and summary bar graphs of activated mouse live, singlet, CD8 $^{+}$  of T cells restimulated for 5 hours with immobilized anti-CD3 and anti-CD28 as indicated after expansion in control (Ctrl) conditions. **B**, Summary flow cytometry bar graphs of CD8 $^{+}$  T cells exposed to the indicated conditions ( $\uparrow$ [K $^+$ ] $_e$  = 40 mmol/L; Gramicidin = 1.5  $\mu$ mol/L). Intracellular [K $^+$ ] is captured by the K $^+$ -sensitive dye APG-4, with relative fluorescence to control conditions. **C** and **D**, Volcano plot depicting comparative expression of loci among CD8 $^{+}$  OT-I naïve (T $_N$ ) and effector memory (T $_{EM}$ ) T cells (**C**) or the impact of 2 hours of TCR ligation in effector T cells (**D**). **E** and **F**, INDEL quantification following CRISPR-Cas9-mediated disruption of the Atp1a1 locus in CD8 $^{+}$  T cells (**E**) and assessment of protein abundance by immunoblot of the same cells (**F**). **G**, Summary bar graphs quantifying [K $^+$ ] $_i$  of CD8 $^{+}$  T cells following CRISPR-Cas9-mediated disruption (Scramble, sgRNA Atp1a1), as indicated by the K $^+$ -sensitive, fluorometric dye APG-4, captured via flow cytometry ( $\uparrow$ [K $^+$ ] $_e$  = 60 mmol/L). Error bars represent standard deviation. \*\*\*, P < 0.005; \*\*\*\*, P < 0.001, two-tailed Student t tests (**A**, **B**, **E**, and **G**).

following Atp1a1 disruption identified signatures canonical for stress response, effector T-cell programs, including mTORC1 and ROS metabolism among others (Supplementary Fig. S1). Consistent with these transcriptional changes, Atp1a1-deficient T cells harbored elevated levels of ROS, quantified by the fluorometric dye DCFDA (Fig. 3C).

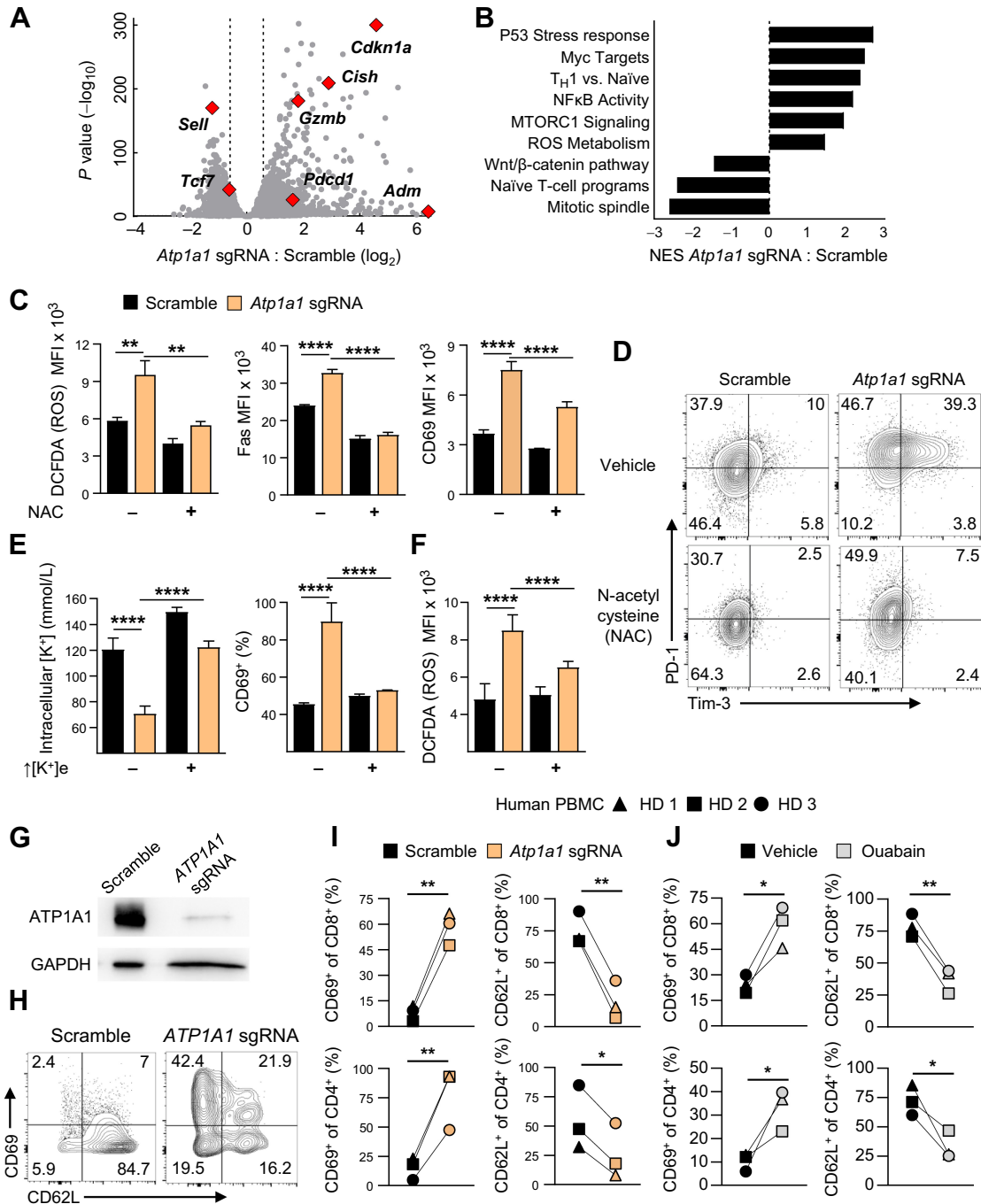
Recent observations that the antioxidant NAC attenuates ROS, limits terminal differentiation, and promotes stemness in T cells prompted us to apply NAC to Atp1a1-deficient T cells in an attempt

to reverse their T $_{Ex}$  cell phenotype (21). Antioxidant-mediated ROS neutralization prevented the accelerated differentiation otherwise observed following Atp1a1 deletion, evidenced by normalization of PD-1, Tim-3, and other markers associated with advanced differentiation, but did not restore cytokine production (Fig. 3C and D; Supplementary Fig. S2A and S2B).

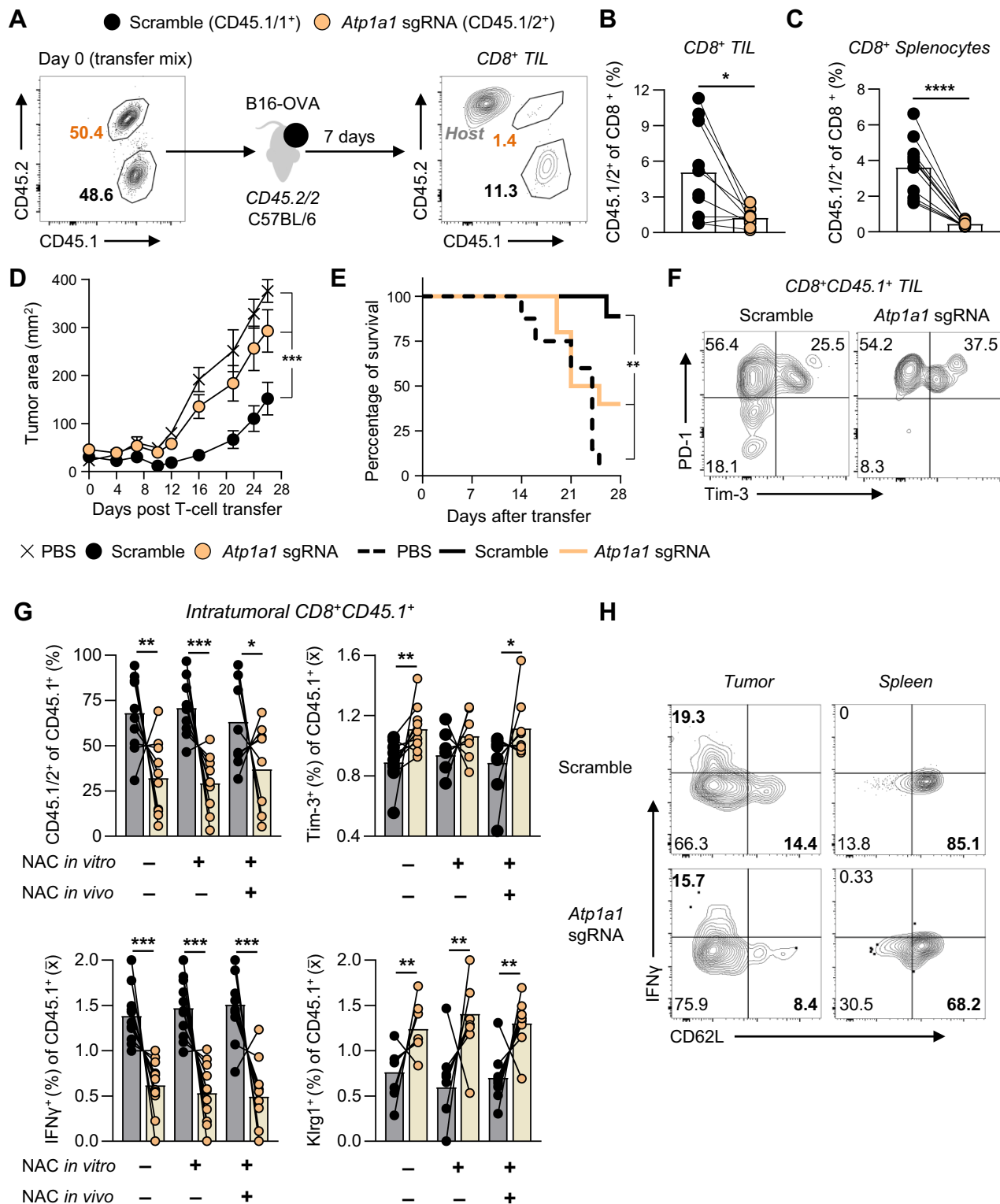
Drawing from our prior observations (Fig. 1A and B; ref. 6), we hypothesized that provision of exogenous K $^+$  could raise [K $^+$ ] $_i$  of Atp1a1-deficient T cells and prevent associated dysfunction. Indeed,

**Figure 2.**

The Na<sup>+</sup>/K<sup>+</sup> ATPase restrains tonic signaling and CD8<sup>+</sup> T-cell dysfunction. **A**, Summary bar graphs quantifying fluorescence of the voltage-sensitive indicator DiSBAC<sub>2</sub>(3), reflecting the transmembrane electrochemical gradient ( $V_m$ ) of CD8<sup>+</sup> T cells in standard RPMI-1640 (Vehicle) or isotonic hyperkalemic conditions (K<sup>+</sup> 20 mmol/L) captured by flow cytometry following CRISPR-Cas9-mediated disruption (Scramble, sgRNA *Atp1a1*) or transduction with retroviral particles. OE, overexpression; DN, Dominant negative. **B** and **C**, Summary quantification of cytoplasmic Ca<sup>2+</sup> as interval Fluo-3/FuraRed fluorescence following TCR cross-linking (**B**) or ionomycin induced store-operated calcium flux (**C**) as indicated, captured by flow cytometry. Iono, Ionomycin.  $n = 3$  technical replicates depicted, representative of two independent experiments. **D**, Representative Phosflow cytometry plots and summary quantification of live, singlet, CD8<sup>+</sup> T-cell populations in the presence or absence of soluble TCR cross-linking stimulation for five minutes. **E**, Concatenated single-cell overlay and colorimetric density tSNE-based depiction of the indicated proteins captured by flow cytometry. **F**, Representative flow cytometry plots and summary quantification for the indicated markers in ex vivo expanded CD8<sup>+</sup> T cells. **G**, Representative and summary quantification of cytokines following acute TCR restimulation of ex vivo expanded CD8<sup>+</sup> T cells. Error bars represent standard deviation. \*,  $P < 0.05$ ; \*\*,  $P < 0.005$ ; \*\*\*\*,  $P < 0.001$ , two-tailed Student *t* tests (**A**, **D**, **F**, and **G**). \*\*\*\*,  $P < 0.001$  for two-way ANOVA (**B** and **C**).

**Figure 3.**

The Na<sup>+</sup>/K<sup>+</sup> ATPase limits T-cell dysfunction by maintaining intracellular [K<sup>+</sup>] and preventing ROS accumulation. **A**, Volcano plot depicting whole-transcriptomic changes in *Atp1a1*-deficient CD8<sup>+</sup> T cells. **B**, Summary GSEA with normalized enrichment scores (NES) for transcripts enriched or lost between indicated groups among the indicated gene-sets. **C**, Summary depiction of reactive oxygen species abundance (quantified by DCFDA fluorescence) and phenotypic surface proteins along with representative flow cytometry plots (D) of effector CD8<sup>+</sup> T-cell populations as indicated ± NAC as in Supplementary Fig. S2A. **E** and **F**, Intracellular potassium concentration (quantified by the K<sup>+</sup>-sensitive dye APG-4) and surface abundance of CD69 quantified by flow cytometry of live, singlet CD8<sup>+</sup> T-cell populations (E) and summary depictions of ROS as quantified by DCFDA during expansion in media supplemented  $\pm \uparrow[K^+]_e$  (40 mmol/L) as in Supplementary Fig. S3A (F). **G**, Immunoblot assessment of ATP1A1 protein abundance in primary human CD3<sup>+</sup> T cells electroporated with scramble sgRNAs or a pool of three *ATP1A1* sgRNAs complexed to spCas9 protein and expanded for 4 days following TCR ligation and IL2 exposure. **H** and **I**, Representative flow cytometry plots and summary analysis of healthy donor CD3<sup>+</sup> T cells as indicated 5 days after electroporation and stimulation as in (G). **J**, Primary human CD3<sup>+</sup> T cells isolated and stimulated via TCR ligation and IL2 as in G-I ± Ouabain (50 nmol/L) for 5 days of culture. Error bars represent standard deviation. \*,  $P < 0.05$ ; \*\*,  $P < 0.01$ ; \*\*\*\*,  $P < 0.0001$  (two-tailed *t* tests). **C–J**,  $n \geq 3$ , each representative of at least two independent experiments.

**Figure 4.**

The Na<sup>+</sup>/K<sup>+</sup> ATPase is required for CD8<sup>+</sup> T-cell persistence and antitumor activity. **A**, Pretransfer flow cytometry of OT-I CD8 T cells electroporated with Cas9 proteins complexed with scramble (CD45.1/1) or *Atp1a1*-targeted (CD45.1/2) sgRNAs mixed at an approximately 1:1 ratio before transfer to C57BL/6 (CD45.2/2) B16-OVA tumor-bearing hosts. **B** and **C**, Representative flow cytometry and summary analysis enumerating live, singlet, CD8<sup>+</sup>, CD8<sup>+</sup> transferred TIL (**B**) and splenocyte populations seven days after transfer to tumor-bearing mice as in **A** (**C**). (Continued on the following page.)

$\uparrow [K^+]_e$  raised  $[K^+]_i$  in *Atp1a1*-deficient T cells, limiting their activation and exhaustion (**Fig. 3E**; Supplementary Fig. S3A). Restoration of  $[K^+]_i$  also limited ROS accumulation in *Atp1a1*-deficient T cells (**Fig. 3F**). These results indicated that  $[K^+]_i$  may have a direct impact on ROS metabolism. Of note, both Scramble and *Atp1a1*-deficient CD8<sup>+</sup> T cells exposed to NAC during their initial activation and expansion acquired a defect in cytokine production (Supplementary Fig. S2B), in line with prior results (21–24). These observations prompted us to interrogate whether  $[K^+]_i$  might influence ROS metabolism following TCR ligation. Indeed, in both serial TCR stimulation and acute TCR stimulation,  $\uparrow [K^+]_e$  limited exhaustion, ROS accumulation, and effector function of CD8<sup>+</sup> T cells (Supplementary Fig. S3B and S3C). Taken together, these results indicate that  $[K^+]_i$  influences ROS metabolism in genetically intact activated T cells, and that suppression of TCR-induced effector function and exhaustion by elevated intracellular K<sup>+</sup> could be mediated through ROS metabolism.

We next asked whether these observations held true in human CD4<sup>+</sup> and CD8<sup>+</sup> T cells. We confirmed CRISPR-Cas9-mediated disruption of ATP1A1 at the protein level via immunoblot following electroporation with Cas9 complexed to ATP1A1 sgRNAs (**Fig. 3G**). Genetic disruption of the Na<sup>+</sup>/K<sup>+</sup> ATPase promoted the retention of the activation marker CD69 and loss of CD62 L in both CD4<sup>+</sup> and CD8<sup>+</sup> T cells (**Fig. 3H** and I). We also found that treatment with the Na<sup>+</sup>/K<sup>+</sup> ATPase inhibitor ouabain during activation and expansion resulted in acquisition of CD69 and loss of CD62 L in CD4<sup>+</sup> and CD8<sup>+</sup> T cells (**Fig. 3J**; refs. 25, 26). These findings indicate that low  $[K^+]_i$  is the primary determinant of T-cell exhaustion in the setting of Na<sup>+</sup>/K<sup>+</sup> ATPase disruption and suggest a link between  $[K^+]_i$  and ROS metabolism. In aggregate, our results suggest that T-cell dysfunction induced by low  $[K^+]_i$  is mediated, in part, by an accumulation of ROS that results in tonic signal transduction.

#### The Na<sup>+</sup>/K<sup>+</sup> ATPase is required for T-cell antitumor activity *in vivo*

To assess the relevance of the Na<sup>+</sup>/K<sup>+</sup> ATPase for T-cell function *in vivo*, we adoptively transferred congenically distinguishable OT-I TCR transgenic CD8<sup>+</sup> T cells following electroporation with Cas9-sgRNA complexes targeting *Atp1a1* or scramble sequences into C57BL/6 mice bearing established B16-OVA subcutaneous melanoma. *Atp1a1*-deletion severely compromised T-cell persistence after adoptive transfer within secondary lymphoid organs and tumors (**Fig. 4A–C**). Demonstrative of their defect in persistence, both tumor regression and host survival were significantly impaired in mice receiving OT-I CD8<sup>+</sup> T cells lacking *Atp1a1* (**Fig. 4D** and E). Phenotypic analysis of transferred populations demonstrated *Atp1a1*-deficient OT-I CD8<sup>+</sup> T cells were in a more exhausted state within the tumor and spleen (**Fig. 4F**; Supplementary Fig. S4A–S4C).

To test whether ROS neutralization could prevent dysfunction and exhaustion of *Atp1a1*-deficient T cells *in vivo*, we again co-transferred CD45.1/2<sup>+</sup> congenically distinguishable OT-I CD8<sup>+</sup> T cells into CD45.2<sup>+</sup> hosts. Despite ongoing exposure to NAC, *Atp1a1*-deficient cells exhibited a similar loss in persistence *in vivo* (**Fig. 4G**; Supplementary Fig. S4D and S4E and S4G and S4H). Ongoing antioxidant provision also failed to augment IFN $\gamma$  production or rejuvenate the T<sub>Ex</sub> cell state of *Atp1a1*-deficient CD8<sup>+</sup> T cells (**Fig. 4G–I**; Supplementary Fig. S4D–S4I). Collectively, these results indicate that the Na<sup>+</sup>/K<sup>+</sup> ATPase plays a critical role in supporting T-cell homeostasis and function by maintaining  $[K^+]_i$  and preventing tonic signal transduction.

## Discussion

The dynamic electrochemical gradients enacted by monovalent ions have been primarily studied for their role in supporting the function of “excitable” cells (i.e., expressing voltage-gated sodium and calcium channels) such as neurons, myocytes, and cardiomyocytes (27, 28). Prior work in T cells has focused on the importance of Kv1.3 and KCa3.1 in maintaining the  $V_m$  to facilitate TCR-induced Ca<sup>2+</sup> influx (9, 29, 30). Others have documented the function of the Na<sup>+</sup>/K<sup>+</sup> ATPase in peripheral T cells, speculating on the dynamics of its function across T-cell subsets and thymocytes (10). We previously reported that  $\uparrow [K^+]_e$  requires PP2A activity to limit Akt-mTOR signaling and effector function in T cells, independent of  $V_m$  and Ca<sup>2+</sup> (6). Here, we again found that the impact of K<sup>+</sup> upon T cells could not be accounted for by Ca<sup>2+</sup> alone. In support of a Ca<sup>2+</sup>-independent role for K<sup>+</sup> is the observation that myeloid cell response to danger signals (inflammasome formation) requires depletion of  $[K^+]_i$  and is also suppressed by  $\uparrow [K^+]_e$  (31). Our observation that restoration of  $[K^+]_i$  normalized ROS levels and T-cell functional state underlines the fundamental, but unexplored, role that  $[K^+]_i$  plays in T-cell function. Although there is a wealth of precedent linking ROS to post-translational modification of signaling machinery, the exact relationship between  $[K^+]_i$  and ROS metabolism remains unclear and warrants additional investigation.

Historically, ROS are considered harmful metabolic by-products that result from mitochondrial activity. More recently, ROS have been appreciated to act as pleiotropic signaling co-factors that control both cellular homeostasis and response to external stimuli (32). Multiple reports have recognized that the influence of ROS in T cells extends to TCR-induced signal transduction, nutrient consumption, and stemness (21–23). Specifically, ROS-mediated oxidation of phosphatase cysteine residues and suppression of their activity has been observed in multiple phosphatases that are central to T-cell function, such as PTP1B, SHP2, PP2A, and PTEN (33). In concert with our prior observations, these findings provide a framework in which  $[K^+]_i$  limits ROS abundance, thus

(Continued.) **D**, Rates of subcutaneous B16-OVA tumor growth represented over time following receipt of OT-I TCR transgenic CD8 T cells electroporated with Cas9 targeted with scramble or *Atp1a1* sgRNAs. **E**, Kaplan-Meier survival estimate of the same cohort as in (D). **F**, Representative flow cytometry of CD45.1 OT-I CD8<sup>+</sup> T cells within B16-OVA tumors, gated as in (B). **G**, Compiled analysis and (H) representative flow cytometry of CD45.1/2 OT-I CD8 T cells isolated and electroporated with sgRNA-Cas9 complexes as indicated and subsequently activated and expanded  $\pm$  NAC *in vitro* (“NAC *in vitro*,” 10 mmol/L). Scramble and *Atp1a1*-deficient cells were then mixed 1:1 and transferred to CD45.2/2 mice bearing established orthotopic B16-OVA tumors, with some receiving daily NAC as indicated. At endpoint, mice received Brefeldin A (protein transport inhibitor) 4–6 hours before euthanasia to capture *in vivo* IFN $\gamma$  production as depicted in Supplementary Fig. S4D. Paired measurements represent the comparative presence per average of the CD45.1<sup>+</sup> T cells in any given mouse for the indicated marker. Two-way ANOVA (D); \*\*\*\*,  $P < 0.0001$ . Two-tailed Student *t* tests (B, C, and G), \*,  $P < 0.05$ ; \*\*,  $P < 0.01$ ; \*\*\*,  $P < 0.001$ . **B–E**,  $n = 10$  mice per group. Representative of two independent experiments. **G**,  $n = 9$ –10 mice per group, data represent two pooled experiments.

maintaining phosphatase activity by preventing their oxidation (1). Taken together, these findings identify a previously unrecognized connection between [K<sup>+</sup>]<sub>I</sub>, ROS homeostasis, and regulation of signal transduction in T cells that warrants further investigation from both a biological and translational perspective.

Although we set out to generate T cells resistant to the ↑[K<sup>+</sup>]<sub>I</sub> within tumors, the ultimate consequence of a persistently low [K<sup>+</sup>]<sub>I</sub> is compromised T-cell antitumor function. However, drawing from the data presented here, we now show that low [K<sup>+</sup>]<sub>I</sub> itself can drive T<sub>EX</sub> cell formation. Thus, the next steps to engineer more effective tumor-specific T cells should include cell-intrinsic approaches to increase ROS neutralization (i.e., viral/ non-viral means to express ROS-neutralizing enzymes in a constitutive or regulable fashion), consideration of viral or non-viral means to augment Na<sup>+</sup>/K<sup>+</sup> ATPase activity with constitutive or regulable expression of ROS producing enzymes (i.e., NAPDH oxidases for cytoplasmic ROS), and *ex vivo* expansion of mouse and human tumor-specific T cells in altered concentrations of [K<sup>+</sup>]<sub>c</sub> to limit activation and exhaustion. Broadly, these findings advance a paradigm, where K<sup>+</sup> transport is central to antitumor function and can be targeted to change T-cell behavior and improve cancer immunotherapies.

## Authors' Disclosures

C. Collier reports grants from AACR, American Society of Clinical Oncology (ASCO), Pancreatic Cancer Action Network, Lyell Immunopharma, and NIH during the conduct of the study. M. McWhorter reports grants from AACR, PanCAN, Lyell

Immunopharma, and NIH during the conduct of the study. C. Jenkins reports grants from AACR, PanCan, ASCO, Lyell, and NIH during the conduct of the study. R. Roychoudhuri reports personal fees from E3DG Genomics, as well as grants from AstraZeneca and F-Star Therapeutics outside the submitted work. R. Eil reports other support from Lyell Immunopharma, as well as grants from American Association of Cancer Research, ASCO, Pancreatic Cancer Action Network, and NIH/NCI (grant no. K08CA256179) during the conduct of the study; and a patent for US 2021/0332326 A1 issued and licensed to Lyell Immunopharma. No disclosures were reported by the other authors.

## Authors' Contributions

**C. Collier:** Conceptualization, data curation, software, formal analysis, validation, investigation, visualization, methodology, writing-original draft, project administration, writing-review and editing. **K. Wucherer:** Conceptualization, validation, investigation, methodology, writing-review and editing. **M. McWhorter:** Formal analysis, investigation, visualization, methodology, writing-review and editing. **C. Jenkins:** Validation, investigation, writing-review and editing. **A. Bartlett:** Conceptualization, formal analysis, investigation, methodology, writing-review and editing. **R. Roychoudhuri:** Conceptualization, methodology, writing-review and editing. **R. Eil:** Conceptualization, resources, data curation, software, formal analysis, supervision, funding acquisition, validation, investigation, visualization, methodology, writing-original draft, project administration, writing-review and editing.

## Note

Supplementary data for this article are available at Cancer Immunology Research Online (<http://cancerimmunolres.aacrjournals.org/>).

Received April 13, 2023; revised September 8, 2023; accepted November 14, 2023; published first xx xx, xxxx.

## References

- Waldman AD, Fritz JM, Lenardo MJ. A guide to cancer immunotherapy: from T-cell basic science to clinical practice. *Nat Rev Immunol* 2020;20:651–68.
- Philip M, Schietinger A. CD8<sup>+</sup> T-cell differentiation and dysfunction in cancer. *Nat Rev Immunol* 2022;22:209–23.
- Sermer D, Batlevi C, Palomba ML, Shah G, Lin RJ, Perales M-A, et al. Outcomes in patients with DLBCL treated with commercial CAR T cells compared with alternate therapies. *Blood Adv* 2020;4:4669–78.
- Wolchok JD, Chiarion-Sileni V, Gonzalez R, Grob J-J, Rutkowski P, Lao CD, et al. Long-term outcomes with nivolumab plus ipilimumab or nivolumab alone versus ipilimumab in patients with advanced melanoma. *J Clin Oncol* 2022;40:127–37.
- Gattinoni L, Klebanoff CA, Restifo NP. Paths to stemness: building the ultimate antitumour T-cell. *Nat Rev Cancer* 2012;12:671–84.
- Eil R, Vodnala SK, Clever D, Klebanoff CA, Sukumar M, Pan JH, et al. Ionic immune suppression within the tumour microenvironment limits T-cell effector function. *Nature* 2016;537:539–43.
- Vodnala SK, Eil R, Kishton RJ, Sukumar M, Yamamoto TN, Ha N-H, et al. T-cell stemness and dysfunction in tumors are triggered by a common mechanism. *Science* 2019;363:eaau0135.
- Ong ST, Ng AS, Ng XR, Zhuang Z, Wong BHS, Prasannan P, et al. Extracellular K<sup>+</sup> dampens T-cell functions: implications for immune suppression in the tumor microenvironment. *bioelectr* 2019;1:169–79.
- Cahalan MD, Chandy KG. The functional network of ion channels in T lymphocytes. *Immunol Rev* 2009;231:59–87.
- Ishida Y, Chused TM. Lack of voltage sensitive potassium channels and generation of membrane potential by sodium potassium ATPase in murine T lymphocytes. *J Immunol* 1993;151:610–20.
- Morth JP, Pedersen BP, Buch-Pedersen MJ, Andersen JP, Vilsen B, Palmgren MG, et al. A structural overview of the plasma membrane Na<sup>+</sup>, K<sup>+</sup>-ATPase, and H<sup>+</sup>-ATPase ion pumps. *Nat Rev Mol Cell Biol* 2010;12:60–70.
- Subramanian A, Tamayo P, Mootha VK, Mukherjee S, Ebert BL, Gillette MA, et al. Gene set enrichment analysis: a knowledge-based approach for interpreting genome-wide expression profiles. *Proc Natl Acad Sci USA* 2005;102:15545–50.
- Liberzon A, Birger C, Thorvaldsdóttir H, Ghandi M, Mesirov JP, Tamayo P. The molecular signatures database (MSigDB) hallmark gene set collection. *Cell Syst* 2015;1:417–25.
- Tan JYW, Folz J, Kopelman R, Wang X. *In vivo* photoacoustic potassium imaging of the tumor microenvironment. *Biomed Opt Express* 2020;11:3507–22.
- Clausen MV, Hilbers F, Poulsen H. The structure and function of the Na, K-ATPase isoforms in health and disease. *Front Physiol* 2017;8:371.
- Blank CU, Haining WN, Held W, Hogan PG, Kallies A, Lugli E, et al. Defining “T-cell exhaustion.” *Nat Rev Immunol* 2019;19:665–74.
- Scott AC, Dündar F, Zumbo P, Chandran SS, Klebanoff CA, Shakiba M, et al. TOX is a critical regulator of tumour-specific T-cell differentiation. *Nature* 2019;571:270–4.
- Long AH, Haso WM, Shern JF, Wanhaninen KM, Murgai M, Ingaramo M, et al. 4-1BB costimulation ameliorates T-cell exhaustion induced by tonic signaling of chimeric antigen receptors. *Nat Med* 2015;21:581–90.
- Pauken KE, Sammons MA, Odorizzi PM, Manne S, Godec J, Khan O, et al. Epigenetic stability of exhausted T cells limits durability of reinvigoration by PD-1 blockade. *Science* 2016;354:1160–5.
- Martinez GJ, Pereira RM, Äijö T, Kim EY, Marangoni F, Pipkin ME, et al. The transcription factor NFAT promotes exhaustion of activated CD8<sup>+</sup> T cells. *Immunity* 2015;42:265–78.
- Pilipow K, Scamardella E, Puccio S, Gautam S, Paoli FD, Mazza EMC, et al. Antioxidant metabolism regulates CD8<sup>+</sup> T memory stem cell formation and antitumor immunity. *JCI Insight* 2018;3:e122299.
- Sena LA, Li S, Jairaman A, Prakriya M, Ezponda T, Hildeman DA, et al. Mitochondria are required for antigen-specific T-cell activation through reactive oxygen species signaling. *Immunity* 2013;38:225–36.
- Jackson SH, Devadas S, Kwon J, Pinto LA, Williams MS. T cells express a phagocyte-type NADPH oxidase that is activated after T-cell receptor stimulation. *Nat Immunol* 2004;5:818–27.

24. Mak TW, Grusdat M, Duncan GS, Dostert C, Nonnenmacher Y, Cox M, et al. Glutathione primes T-cell metabolism for inflammation. *Immunity* 2017;46: 675–89.
25. Lowery FJ, Krishna S, Yossef R, Parikh NB, Chatani PD, Zacharakis N, et al. Molecular signatures of antitumor neoantigen-reactive T cells from metastatic human cancers. *Science* 2022;375:877–84.
26. Krishna S, Lowery FJ, Copeland AR, Bahadiroglu E, Mukherjee R, Jia L, et al. Stem-like CD8 T cells mediate response of adoptive cell immunotherapy against human cancer. *Science* 2020;370:1328–34.
27. Burke KJ Jr, Bender KJ. Modulation of ion channels in the axon: mechanisms and function. *Front Cell Neurosci* 2019;13:221.
28. Grant AO. Cardiac ion channels. *Circ Arrhythm Electrophysiol* 2009;2:185–94.
29. Feske S, Skolnik EY, Prakriya M. Ion channels and transporters in lymphocyte function and immunity. *Nat Rev Immunol* 2012;12:532–47.
30. Feske S, Wulff H, Skolnik EY. Ion Channels in innate and adaptive immunity. *Annu Rev Immunol* 2015;33:291–353.
31. He Y, Zeng MY, Yang D, Motro B, Núñez G. NEK7 is an essential mediator of NLRP3 activation downstream of potassium efflux. *Nature* 2016;530: 354–7.
32. Niethammer P, Grabher C, Look AT, Mitchison TJ. A tissue-scale gradient of hydrogen peroxide mediates rapid wound detection in zebrafish. *Nature* 2009; 459:996–9.
33. Finkel T. Signal transduction by reactive oxygen species. *J Cell Biol* 2011;194: 7–15.